April 2009 *Volume 5 Issue 2*

Trade Science Inc.

Materials Science

An Indian Journal

Full Paper

MSAIJ, 5(2), 2009 [122-130]

Theoretical calculations of structural, electronic and optical properties of $Ca_xZn_{1-x}S$ alloys

Bin Amin[1], Safdar Nazir[2], Nazma Ikram[2], Iftikhar Ahmad[1]*, Yasir Saeed[3], Suneela Arif[1]

[1]Department of Physics, Hazara University, Garden Campus, Mansehra, (PAKISTAN)

[2]CSSP, Quaid-e-Azam Campus, Punjab University, Lahore, (PAKISTAN)

[3]Department of Physics, G.C. University, Faisalabad, (PAKISTAN)

Phone : (092)-997-414132

E-mail : peacetopeace@gmail.com

Received: 12th February, 2009 ; Accepted: 17th February, 2009

ABSTRACT

The structural, electronic and optical properties of $Ca_xZn_{1-x}S$ in B3 phase are investigated in order to see the effect of addition of Ca in ZnS in the range $0 \leq x \leq 1$. For this purpose, first principle density functional calculations, using full potential linearized augmented plane wave (FP-LAPW) method, have been used. The equilibrium structural parameters for $Ca_xZn_{1-x}S$ are obtained from the total energy minimization calculations with respect to volume. The electronic structure and the density of states for $Ca_xZn_{1-x}S$ are calculated and analyzed in terms of the contribution of Zn s and d, S s and Ca p and d states. Optical properties such as complex dielectric constants (ε), refractive index (n), extinction coefficient (k), normal-incidence reflectivity (R), absorption coefficient (α), and optical conductivity (σ), are also calculated and analyzed in the incident photon energy range 0-50 eV. It is found that the direct bandgap $E_g^{\Gamma-\Gamma}$ varies from 2.2 eV to 3.7 eV as x varies from 0 to 1 and the optical properties of $Ca_xZn_{1-x}S$ also changes accordingly.

KEYWORDS

Metal oxides;
Electronic structure;
Optical properties;
Band structure;
Theoretical calculation.

1. INTRODUCTION

Technological and theoretical interests in the wide band gap II-VI compounds and their alloys have been growing recently due to their use in electro-optical and electron-acoustic devices[1]. The II-VI compounds are promising materials for light emitting devices which operate in the blue to ultraviolet region. Recent progress in the blue laser diodes (LDs) and full-color electroluminescent (EL) displays has evoked a strong interest in the study of these materials[2].

ZnS is a prototype II-VI wide band gap semiconductor and its cubic phase occurs naturally as a mineral is called the zinc-blend (ZB) structure. The ZnS crystal also exists in wurtzite structure. The wurtzite structure is different from the zinc-blend structure at the relative position of the third neighbor and beyond. The local atomic environments in both crystals are sufficiently close and it has been taken for granted that their electronic structures should also be very similar. In comparison with wurtzite structure, very little is known about the electronic, optical and mechanical properties of zinc-

blend II-VI group under high pressure and temperature. Moreover the zinc-blend phase is expected to be more amenable to doping than the wurtizite phase. Recently an investigation on the pressure induced transformation of nano-crystalline ZnS was carried out by Pan et al.[3] using an energy dispersive X-ray diffraction technique and they reported the transformation from wurtzite to ZB at 11.5 GPa and then to rocksalt (RS) structure at 16 GPa.

Crystalline zinc sulphide (ZnS) is widely applied in electroluminescent devices, blue or ultra violet light emitting diodes, laser diodes and tuneable mid infrared lasers and second harmonic generation devices[4]. Crystalline ZnS thin films can be prepared by conventional deposition techniques such as liquid or vapor phase epitaxy. Due to low growth temperature and low kinetic energy of the transporting molecules in conventional epitaxy, crystalline ZnS grown on various substrates is normally of zinc-blend structure and poor crystalline quality. Considerable efforts are being devoted to realize a p-type material by doping or growing ZnS with impurities such as Li or Cl. When doped with Mn, the Zn based wurtzite crystal forms an interesting group of dilute magnetic semiconductors.

Calcium sulphide, like other alkaline-earth sulphides, has recently attracted increasing interests because of its potential technological use, particularly as host material for device application ranging from photo- and electroluminescent thin films to magneto-optical devices, owing to its wide band gap[5,6]. Chen et al.[7] have calculated the structural and electronic properties of CaS compound in all four B1, B2, B3 (zinc-blend) and B4 (wurtzite) phases, using DACAPO code with the GGA approximation using ultra-soft pseudopotential[8]. They found that only B2 phase of CaS has an indirect band gap, while all the other three phases are direct band-gap materials. Experimental reflectivity spectrum studies of Kaneko et al.[9] and optical absorption spectrum studies by Jin et al.[10] indicates that B1 phase have indirect band gap (Γ-X) of 4.434 eV and 4.52 eV and direct band-gap (Γ-Γ) of 5.343 eV and 5.33 eV. An earlier optical absorption measurement in CaS yielded a band-gap value of 5.38 eV; however the nature of the band gap remained unclear[11]. The theoretical result of Chen et al.[7] are not only contrary to these experimental studies as regard to the nature of the band gap[12], there seems to be inconsistencies between the band structures of the different phases of CaS and their respective density of states (DOS) plots.

In this paper the structural, electronic and optical properties for $Ca_xZn_{1-x}S$ ternary alloy in B3 phase at different concentrations of Ca are calculated; by using the full potential linearized augmented plane wave (FP-LAPW) method in the frame work of density functional theory. Equilibrium volume, bulk modulus, direct band-gap $E_g^{\Gamma-\Gamma}$, dielectric constants (ε), refractive index (n), extinction coefficient (k) and normal incident reflectivity are calculated and compared with other calculated and experimental results.

2. Computational details

First principle band structure calculations for $Ca_xZn_{1-x}S$ within the frame work of density functional theory with the localized density approximation (LDA) using the Wu-Cohen exchange-correlation potential[13] have been performed. The Kohn-Sham equations were solved with the full potential linear augmented plane wave (FP-LAPW) technique, using the WIEN2K package[14]. In the present self-consistent calculations, a muffin-tin model for the crystal potential is assumed and the unit cell is divided into two regions, within and outside the muffin-tin. The electrons are paired into two groups, namely the core electrons whose charge densities are confined within the muffin-tin spheres and the valence electrons. The core electron states are treated fully relativistically by solving the Dirac equation, whereas the valence electrons are treated non-relativistically. In both regions of the unit cell, different basis sets are used to expand the wave function. Inside the non-overlapping spheres of muffin-tin around each atom, linear combination of radial solution of the Schrödinger equation times the spherical harmonic is used whereas the plane wave basis set is used in the interstitial region. The muffin-tin radius R_{MT} is chosen such that there is no charge leakage from the core and total energy convergence is ensured. R_{MT} values of 2.4, 2.26, 2.12 a.u are used for Zn, Ca and S respectively. The maximum value of angular momentum $l_{max} = 10$ is taken for the wave function expansion inside the atomic spheres. For plane wave expansion of the electron wave function in the interstitial region for $Ca_xZn_{1-x}S$, the plane

Full Paper

wave cut-off value of $K_{max} \times R_{MT} = 9$ is used, while for the binary compounds (ZnS, CaS) $K_{max} \times R_{MT} = 8$ is used. A mesh of 72 k - points for the binary compounds are taken for the Brillouin zone integrations in the corresponding irreducible wedge. A finer k mesh is required for the evaluation of complex dielectric constant and other related optical properties. We have used 3500 k - points in the calculations of optical properties.

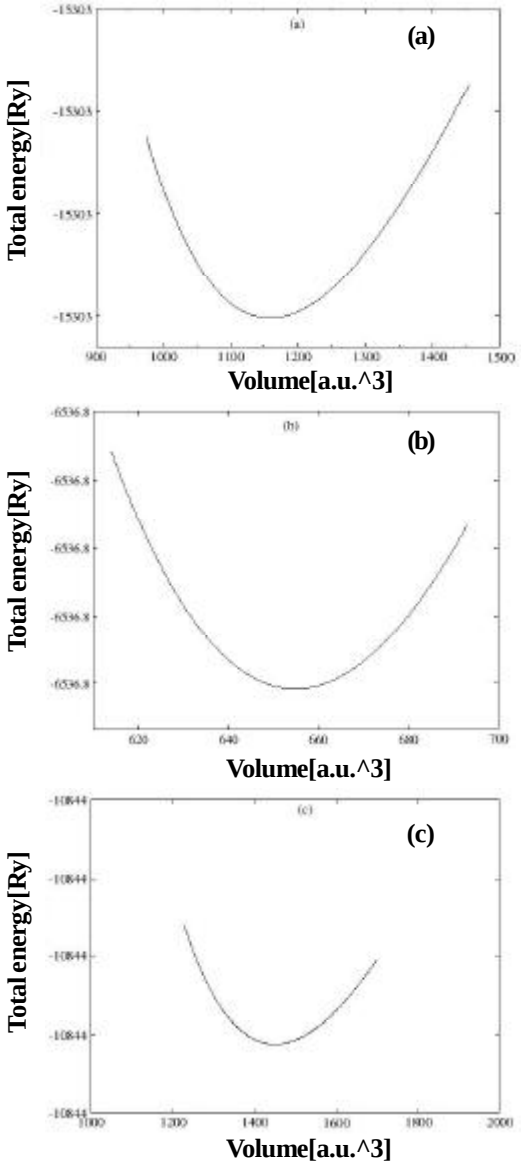

Figure 1: Variation of total energy[Ry] as a function of volume[a.u.^3] for (a) $Ca_{0.25}Zn_{0.75}S$, (b) $Ca_{0.50}Zn_{0.50}S$ and (c) $Ca_{0.75}Zn_{0.25}S$

3. RESULTS AND DISCUSSIONS

3.1. Structural properties

In order to study the structural properties of the ternary alloys $Ca_xZn_{1-x}S$ for x = 0, 0.25, 0.50, 0.75 and 1, the structural properties of the binary compounds ZnS and CaS are calculated in B3 phase. For each composition, volume optimization is performed by minimizing the total energy with respect to the unit cell volume using the Murnaghan's equation of state[15] and the minimum volume is noted figure 1. Next the equilibrium structural parameters such as the lattice constant a and the bulk moduli B are evaluated. It is found that the values of lattice constant and bulk modulus with LDA are in good agreement with the experimental and other calculated values, TABLE 1.

The equilibrium lattice constant and bulk moduli for $Ca_xZn_{1-x}S$ alloys as function of x are presented in figures 2 and 3. It is noticed that, the calculated lattice

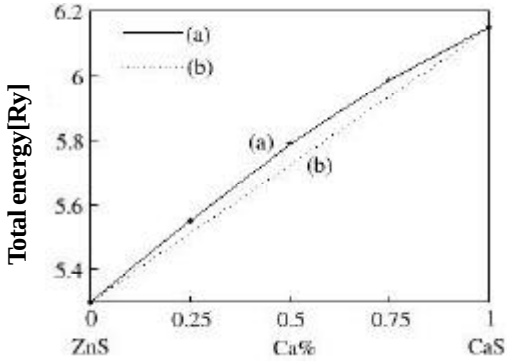

Figure 2: (a) The calculated lattice constant as a function of x for $Ca_xZn_{1-x}S$; ——— (b) Vegard's law - - - - - -

TABLE 1: Calculated lattice constants and bulk moduli of $Ca_xZn_{1-x}S$ compared to experimental and other theoretical results

	Lattice Constant a(A^0)			Bulk Moduli B(GPa)		
X	This work	Exp	Other calc	This work	Exp	Other calc
0	5.30	5.41[a]	5.3998[b], 5.580[c], 5.280[d]	86.01	76.9[a], 83.1[e]	80.97[b], 75.9[c], 83.3[d]
0.25	5.55			65.98		
0.50	5.79			53.10		
0.75	5.99			48.25		
1	6.15		6.0[f], 6.12[g], 6.294[h]	45.0172		43.6[f],47[g], 40.86[h]

[a]Ref.[16,17], [b]Ref.[18], [c]Ref.[19], [d]Ref.[20], [e]Ref.[21], [f]Ref.[22], [g]Ref.[23], [h]Ref.[24]

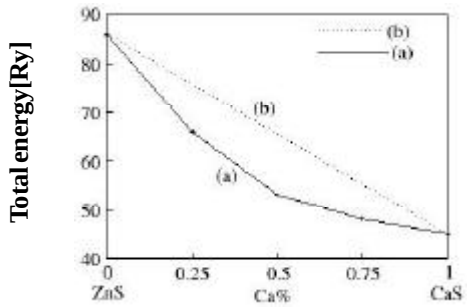

Figure 3: (a) The calculated bulk Moduli as a function of χ for $Ca_xZn_{1-x}S$; ——(b) Vegard's law - - - - - -

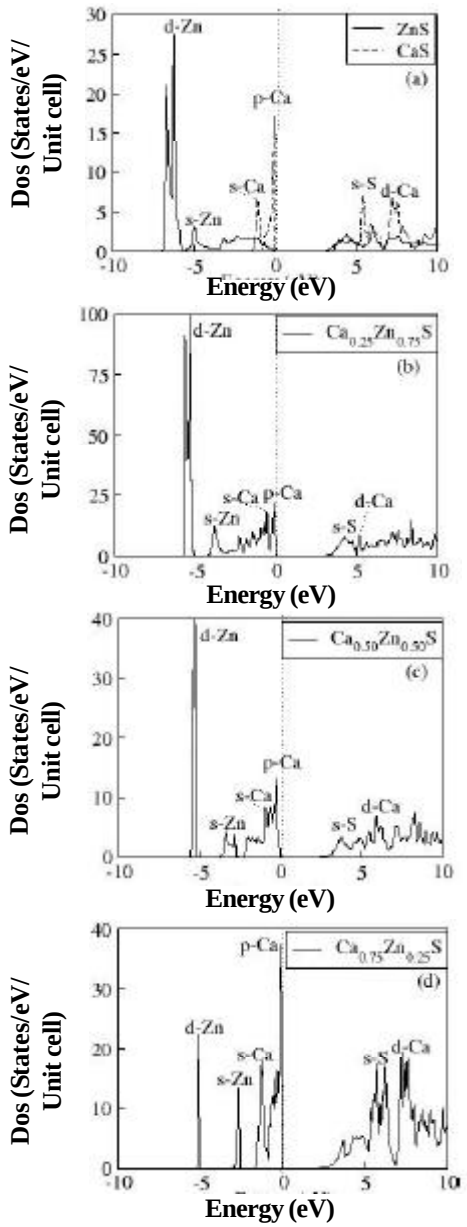

Figure 4: TDOS (a) ZnS and CaS (b) $Ca_{0.25}Zn_{0.75}S$ (c) $Ca_{0.50}Zn_{0.50}S$ and (d) $Ca_{0.75}Zn_{0.25}S$

TABLE 2: Direct band-gap energy (eV) of $Ca_xZn_{1-x}S$ alloys at different Ca concentrations

X	$E_g^{\Gamma-\Gamma}$ (eV)		
	This work	Exp	Other calc
0	2.2	3.53[a], 3.4[b]	3.74[c], 3.73[c]
0.25	2.8		
0.50	2.9		
0.75	3.2		
1	3.7		3.4[d], 3.18[e]

[a]Ref.[25], [b]Ref.[26], [c]Ref.[27], [d]Ref.[28], [e]Ref.[24]

constants followed the vegard's law. Whereas the bulk modulus shows considerable bowing and obey the equation,

$$B(x) = 85.56 - 87.45x + 47.57x^2 \quad (1)$$

Electronic properties

The band structures and density of states for B3 phase of $Ca_xZn_{1-x}S$ corresponding to x = 0, 0.25, 0.50, 0.75 and 1 are calculated, using the FP-LAPW approach with LDA scheme. Figure 4 shows the total density of states (TDOS) along with the Ca p and s, Zn d and s and S s partial density of states (PDOS) of $Ca_xZn_{1-x}S$ compound. The contribution of s, p and d states of Zn, Ca and S are observed.

In ZnS, Zn 3d state gives the major contribution in the valance band, whereas in CaS, Ca 3p state plays the pivotal role in the valance band and S 3s state in the conduction band. When the ternary compound is formed, the lower part of the valance band is totally dominated by Zn 3d state and the upper part of the valance band is totally dominated by Zn 4s and Ca 3p states, while the lower part of the conduction band is dominated by S 3s and upper part by Ca 3d state for all concentrations of Ca. The position of peaks Zn-d and s Ca-d and S-s remain the same, but their contribution varies.

For the electronic band structure calculations, the, Zn 3d and 4s Ca 3p, and 4s and S 3s and 3p states are taken as valence states and all lower lying states are treated as part of the core. The band structure of $Ca_xZn_{1-x}S$ is calculated for x = 0, 0.25, 0.5, 0.75 and 1. It is observed that ZnS (x=0) and CaS (x=1) are direct band gap materials in B3 phase with the band gaps $E_g^{\Gamma-\Gamma}$ values of 2.2 eV and 3.7 eV respectively. The band structure of $Ca_xZn_{1-x}S$ for x= 0.25, 0.50 and 0.75 are shown in Figure 5 along high symmetry direc-

Full Paper

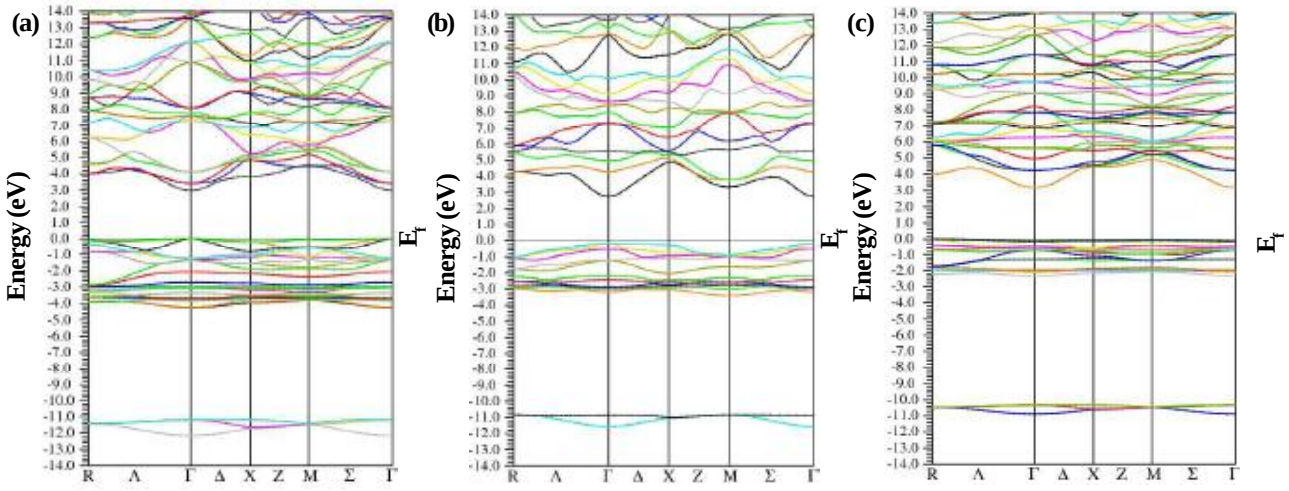

Figure 5: Band structure (a) $Ca_{0.25}Zn_{0.75}S$ (b) $Ca_{0.50}Zn_{0.50}S$ and (c) $Ca_{0.75}Zn_{0.25}S$

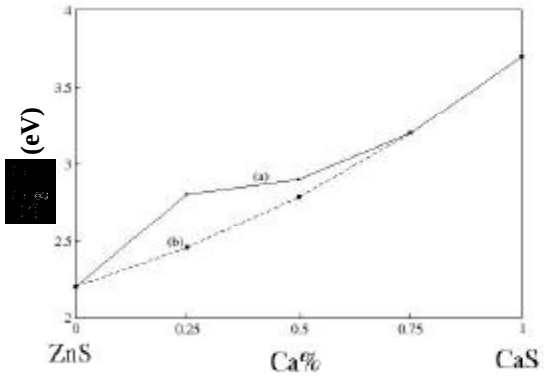

Figure 6: $E_g^{\Gamma-\Gamma}$ as a function of x, (a) calculated values (b) electronegativity expression

tions and the calculated values for $E_g^{\Gamma-\Gamma}$ at different x are compared with experimental data and with other calculations, TABLE 2.

Figure 6 shows the direct band gaps of $Ca_xZn_{1-x}S$ as a function of composition x. It is found that the direct band gap changes according to $E_g^{\Gamma-\Gamma} = 2.9\text{-}0.8x + 1.6x^2$ in the range $0.25 \leq \times 1$. The calculated values of $E_g^{\Gamma-\Gamma}$ are also compared with electronegativity equation (2).

$$E_g^{Ca_xZn_{1-x}S} = xE_g^{CaS} + (1-x)E_g^{ZnS} - \Delta\chi \times x(1-x) \qquad (2)$$

Where $\Delta\chi$ represents the electronegativity difference between Zn and Ca cations. The calculated value of $E_g^{\Gamma-\Gamma}$ shows considerable deviation from the electronegativity equation around x= 0.25. It is due to the fact that in the density of states for the binary alloy ZnS, Zn has *d* and *s* states at -6.51 eV and -4.95 eV respectively.

When Ca is added the Ca s and p states lay close to the Fermi surface, that is, in the energy range -1.03 eV and -0.39 eV. Hence Ca plays an important role in the ternary alloy $Ca_xZn_{1-x}S$. The same behavior was observed in $Ca_xZn_{1-x}O$, where in the valence band the Op state was close to the Fermi surface, with the addition of Ca in ZnO, the Ca p state also located itself near the Fermi surface.

Optical properties

3.3.1. Dielectric function

In order to study the optical properties of $Ca_xZn_{1-x}S$, it is necessary to investigate the complex dielectric function $\varepsilon(\omega)$ which gives the response of the solid to electromagnetic radiations. Other properties such as refractive index, extinction coefficient and reflectivity are related to $\varepsilon(\omega)$.

The imaginary part of the frequency dependent dielectric function $\varepsilon_2(\omega)$ for structures with cubic symmetry is given by

$$\varepsilon_2(\omega) = \frac{8}{2\pi\omega^2}\sum_{nn'}\int_{BZ}|P_{nn'}(k)|^2\frac{dS_k}{\nabla\omega_{nn'}(k)}$$

$\varepsilon_2(\omega)$ is strongly related to the joint density of the states (DOS) $\omega_{nm'}$ and momentum matrix element $P_{m'}$. The real part of the dielectric function $\varepsilon_1(\omega)$ is obtained from $\varepsilon_2(\omega)$ by using the Kramers-Kronig relations[29],

$$\varepsilon_1(\omega) = 1 + \frac{2}{\pi}P\int_0^\infty \frac{\omega'\varepsilon_2(\omega')}{\omega'^2-\omega^2}d\omega'$$

Optical parameters of the alloys were calculated

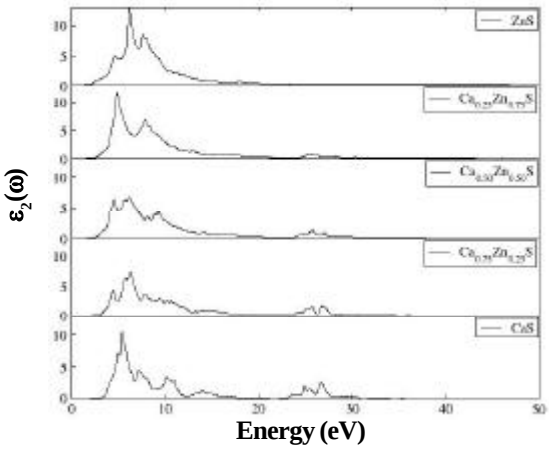

Figure 7: $\varepsilon_2(\omega)$ for $Ca_xZn_{1-x}S$ corresponding to different values of x

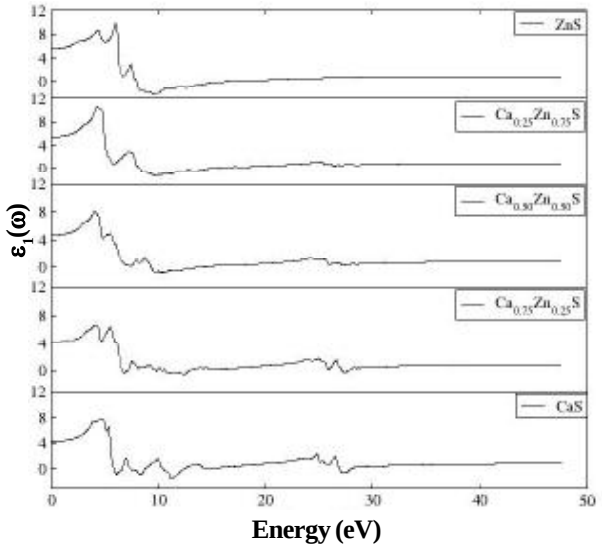

Figure 8: $\varepsilon_1(\omega)$ for $Ca_xZn_{1-x}S$ corresponding to different values of x

TABLE 3: Calculated optical parameters of $Ca_xZn_{1-x}S$ alloys at different Ca concentrations

x	$E_g^{\Gamma-\Gamma}$ (eV)	$\varepsilon_1(0)$	$\varepsilon_2(\omega)$	$n(\omega)$	$k(\omega)$	$R(\omega)$	$\alpha(\omega)$	$\sigma(\omega)$
0	2.2	5.78	2.13	2.45	2.22	0.17	2.5	2.4
0.25	2.8	5.45	2.66	2.32	2.65	0.16	2.8	2.8
0.50	2.9	4.75	2.75	2.20	2.75	0.14	3.01	2.9
0.75	3.2	4.16	3.01	2.14	3.01	0.12	3.27	3.2
1	3.7	4.12	3.28	2.12	3.20	0.11	3.62	3.6

using 3500 k points in the irreducible Brillouin zone (BZ).

The calculated imaginary parts of the dielectric function for $Ca_xZn_{1-x}S$ for x = 0, 0.25, 0.50, 0.75 and 1 are shown in figure 7. The critical points in $\varepsilon_2(\omega)$ occur at about 2.13 eV, 2.66 eV, 2.75 eV, 3.01 eV and 3.28 eV corresponding to x=0, 0.25, 0.50, 0.50, 0.75 and respectively and are attributed to the threshold for the direct optical transitions occurring at 2.2 eV, 2.8 eV, 2.9 eV, 3.2 eV and 3.7 eV respectively.

It is observed that the overall behavior of $\varepsilon_2(\omega)$ appears to be similar for all concentrations of Ca with some difference in details. It is noted that the binary alloy ZnS has a strong absorption region in the range 2.3 eV-14.8 eV, whereas CaS has two regions of strong absorption, i.e., in the range 3.54 eV-15.26 eV and 23.37 eV-27.87 eV. In these energy ranges, $\varepsilon_1(\omega)$ goes from maximum to minimum and these features are also reflected in the ternary alloys.

In figure 8 we present our calculated real part of the dielectric function and report the main optical transition energies (eV). The most important quantity of $\varepsilon_1(\omega)$ is the zero frequency limit $\varepsilon_1(0)$, which is the electronic part of the static dielectric constant that depends strongly on the band gap. This quantity may be related to the refractive index $n(\omega) = \sqrt{\varepsilon_1(0)}$

Our calculated static dielectric constants for $Ca_xZn_{1-x}S$ are 5.78, 5.45, 4.75, 4.16 and 4.12 corresponding to *x* = 0, 0.25, 0.50, 0.75 and 1. The corresponding values of $E_g^{\Gamma-\Gamma}$ are 2.2 eV, 2.8 eV, 2.9 eV, 3.2 eV and 3.7 eV respectively. It is noticed that a smaller energy gap yields a larger $\varepsilon_1(0)$. Decrease in the dielectric function with the increase of optical energy gap has also been observed in the recent experiments on SiOC films by Yu et al.[30]. It is found that in the ZnS, there is a shoulder at 2.13 eV and in CaS a distinct peak is observed at 3.72 eV corresponding to the direct band gaps in these binary alloys, TABLE 3. As Ca is added in ZnS the shoulder shifts towards higher energies.

3.3.2. Refractive index and reflectivity

From (ω), other important optical constants for practical-device engineering are evaluated, such as the refractive index $\tilde{n}(\omega)$ including extinction coefficient k (ω) and normal-incidence reflectivity R (ω).

The refractive indices of ternary alloys are important optical design parameters, e.g. for distributed Bragg reflectors (DBRs) in vertical cavity surface emitting lasers[31]. The complex refractive index is given by

$$\tilde{n} = n + ik = \varepsilon^{1/2} = (\varepsilon_1 + i\varepsilon_2)^{1/2}$$

where n represents the real part of the refractive index and k is the extinction-coefficient. We can determine the refractive in-

Full Paper

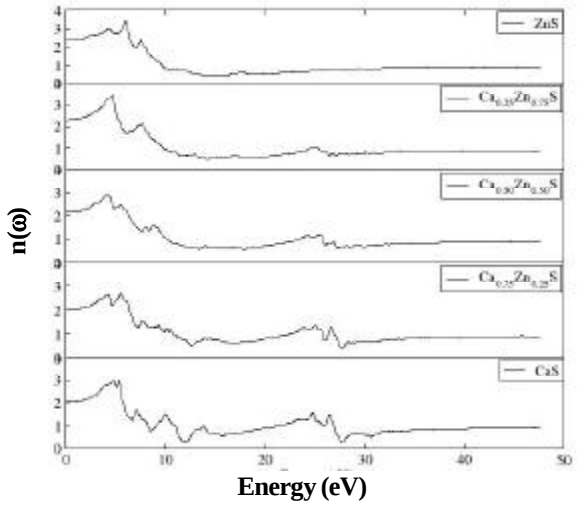

Figure 9: Refractive index n (ω) of $Ca_xZn_{1-x}S$ corresponding to different values of x

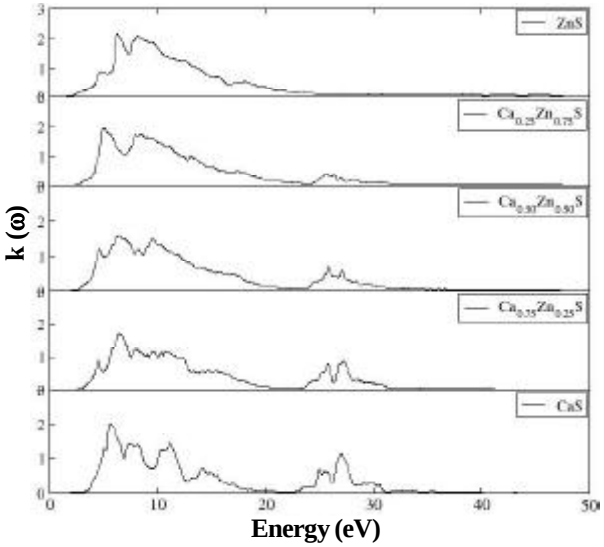

Figure 9: Refractive index n (ω) of $Ca_xZn_{1-x}S$ corresponding to different values of x

dex n(ω) and extinction coefficient k (ω) from the relations.

$$\mathbf{n(\omega)=\frac{1}{\sqrt{2}}\left[\left\{\varepsilon_1(\omega)^2+\varepsilon_2(\omega)^2\right\}^{1/2}+\varepsilon_1(\omega)\right]}$$

$$\mathbf{k(\omega)=\frac{1}{\sqrt{2}}\left[\left\{\varepsilon_1(\omega)^2+\varepsilon_2(\omega)^2\right\}^{1/2}-\varepsilon_1(\omega)\right]}$$

The graphs of n(ω) and k(ω) have been displayed in figures 9 and 10 respectively. It can be seen from these figures that n(ω) closely follows $\varepsilon_1(\omega)$, whereas k(ω) changes as $\varepsilon_2(\omega)$.

From the refractive index and extinction coefficients we can calculate the normal-incidence reflectivity by using the equation

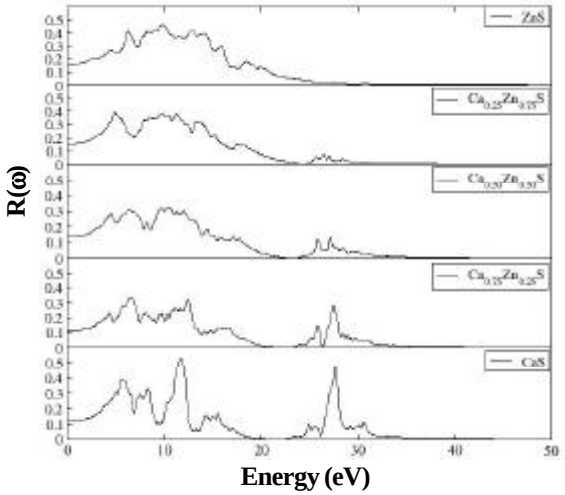

Figure 11: Reflectivity R (ω) for $Ca_xZn_{1-x}S$ corresponding to different values of x

$$\mathbf{R(\omega)=\left|\frac{\tilde{n}-1}{\tilde{n}+1}\right|=\frac{(n-1)^2+k^2}{(n+1)^2+k^2}}$$

The normal incident reflectivity gives good information about different critical points of transition. Figure 11 shows the reflectivity spectra. The reflectivity region for ZnS is in the energy range of 4.41 eV-25.09 eV and corresponds to the frequency range 6.7×10^{15} rad sec^{-1}-3.8×10^{16} rad sec^{-1}.

It is observed that in CaS the reflectivity spectra R (ω) has two regions. The first region is in the energy range 3.01 eV - 18.14 eV, which corresponds to the frequency range 4.57×10^{15}– 2.75×10^{16} rad sec^{-1}. The second reflectivity region is from 23.33 eV-33.72 eV and corresponds to frequencies 3.5410^{16} rad sec^{-1}-5.12×10^{16} rad sec^{-1}. These regions are reflected in the ternary alloys. All these reflectivity regions belong to UV region of the electromagnetic spectrum. As the Ca concentration decreases in $Ca_xZn_{1-x}S$ the second reflectivity region diminishes till it vanishes in ZnS.

3.3.3. Absorption-coefficient and optical conductivity

Our calculations of absorption coefficient α(ω) and optical conductivity σ (ω) for $Ca_xZn_{1-x}S$ corresponding to x=0, 0.25, 0.50, 0.75 and 1 are shown in figures 12 and 13 respectively.

It is noticed that there is a high absorption region in ZnS in the energy range 4.15 eV-21.15 eV. As the concentration of Ca is increased this absorption region shifts

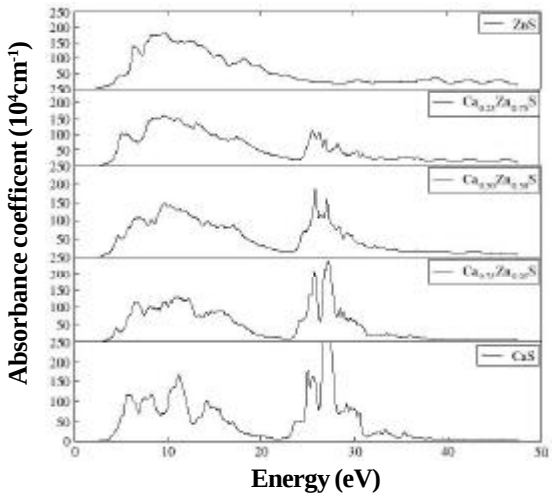

Figure 12: Absorption coefficient α(ω) for $Ca_xZn_{1-x}S$ corresponding different values of x

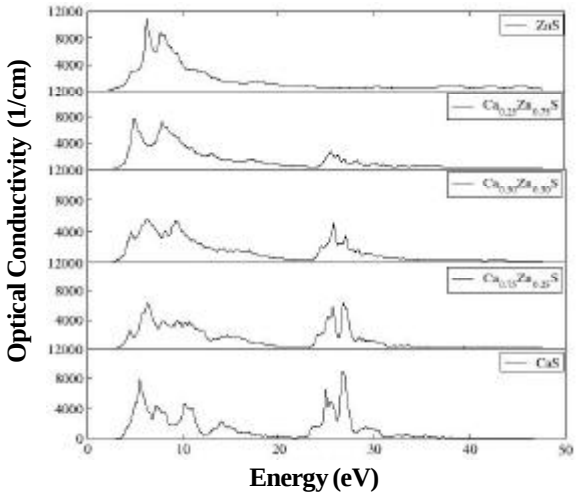

Figure 13: Optical Conductivity σ (ω) for $Ca_xZn_{1-x}S$ corresponding different values of x

towards the higher energies. In CaS, $\varepsilon_1(\omega)$ is negative in the range 5.67 eV-6.73 eV, 7.96 eV-8.76 eV, 10.52 eV-12.38 eV and 26.8-28.0 eV. The absorption co-efficient shows peaks in the region 5.30 eV-6.87 eV, 7.14 eV-8.63 eV 10.04 eV-12.32 eV and 26.1-28.23 eV. Further, the reflection co-efficient of CaS passes through maxima in the range 5.1 eV-6.53 eV, 7.93 eV-8.55 eV, 10.49 eV-12.42 eV and 26.50 eV-28.35 eV.

Hence when Ca concentration is increased from 0 to 1 the absorption and reflection coefficients show features observed in CaS plots. Since the optical conductivity σ(ω) is proportional to $\varepsilon_2\omega$, the conductivity curve follows the pattern of $\varepsilon_2(\omega)$ with sharper peaks at higher ω.

4. CONCLUSION

The full potential linearized augmented plane wave (FP-LAPW) method in the wien2k code has been used to study the structural, electronic and optical properties of $Ca_xZn_{1-x}S$ in B3 phase. It is found that the lattice constant deviates slightly from linearity whereas the bulk modulus shows considerable bowing as a function of the calcium concentration. The calculations of density of states and band structure for various compositions of $Ca_xZn_{1-x}S$ show that the lower part of the valance band is dominated by the Zn 3d and 4s states and the upper part of the valance band has Ca 3p states whereas Ca 3d and S 2s states prevail in the upper part of the conduction band. It is further found that in the ternary alloy the position of these states remains the same however their magnitude varies in accordance with the concentration of Zn and Ca. Next, the dependence of band gap $E_g^{\Gamma-\Gamma}$ in $Ca_xZn_{1-x}S$ as a function of x is evaluated. It is observed that the calculated values of direct band gap around x= 0.25 is different from the corresponding value given by the empirical relation. This deviation is attributed to the fact that Zn belongs to VIb group and Zn d state lies deep in the valence band whereas Ca belongs to IIa group and its 3p state lies close to the Fermi surface hence its effect on the band structure is prominent. So for no experimental work has been done on the ternary alloy $Ca_xZn_{1-x}S$, but since the direct bandgap of this alloy varies from 2.2 eV to 3.7 eV as x changes from 0 to 1, it can be used as a potential material for devices which work in the UV region of the spectrum. The results of optical properties also show that $Ca_xZn_{1-x}S$ can be efficiently used in devices working in the UV range.

5. REFERENCES

[1] F.Benkabou, H.Aourag, M.Certier; Material Chemstry and Physics, **66**, 10 **(2000)**.

[2] S.T.Lee, M.Ktagawa, R.Suzukawa, K.Ichino, H.Kobayshi; Journal of Crystal Growth **154**, 399 **(1995)**.

[3] Y.Pan, S.Qu, S.Dong, Q.Cw, W.Zhang, X.Liu, J.Liu, C.Gao, G.Zou; J.Phys.Condense matter, **14**, 10484 **(2002)**.

[4] Z.J.Xin, R.Peaty, H.N.Rutt, R.W.Eason, Semicon-

ductor Science and Technology, **14**, 695 (**1999**).
[5] R.P.Rao; J.Matter.Sci., **5**, 3357 **(1986)**.
[6] S.Hakamata, M.Ehara, H.Kominami, Y.Nakanishi, Y.Hatanaka; Applied Surface Sciences, **244**, 469 **(2005)**.
[7] Z.J.Chen, H.Y.Xiaa, X.T.Zua; Physica.B, **391**, 193 **(2007)**.
[8] Dacapo Version 2.7, http//www.fysik.dtu.dk/CAMPOS/
[9] Y.Kaneko, T.Koda; J.Cryst.Growth, **86**, 72 **(1988)**; Y.Kaneko, K.Morimoto, T.Koda; J.Phys.Soc. Japan, **52**, 4385 (**1983**).
[10] M.S.Jin, N.O.Kim, C.S.Yoon, C.I.Lee, M.Y.Kim, W.T.Kim; J.Korean Phys.Soc., **39**, 692 **(2001)**.
[11] G.A.Saum, E.B.Hensley; Phys.Rev., **113**, 1019 **(1959)**.
[12] Z.J.Chen, H.Y.Xiao, X.T.Zu; Physica B, **391**, 193 **(2007)**.
[13] Z.Wu, R.E.Cohen; Phys.Rev.B, **73**, 235116 **(2006)**.
[14] P.Bhala, K.Schwarz, G.K.H.Madsen, D.Kvanicka, J.Luitz; WIEN2K, An Augmented plane wave+Local Orbital Program for Calculating Crystal Properties Karlheinz Schwarz, Techn. Universitat, Wien, Austria. ISBN: 3-9501031-1-1-2 **(2001)**.
[15] F.D.Murnaghan; Proc.Natl.Acad.Sci. USA, **30**, 244 **(1994)**.
[16] O.Mandelung; 'Physics of II-IV and I-VII Compounds, Semimagnetic Semiconductors, Landalt Bornstein New Series group III', Springer, Berlin 7, **(1982)**.
[17] K.H.Hellwege, O.Mandelung; 'Semiconductors, Intrinsic Properties of Group IV Elements and III-V, II-VI and I-VII Compunds', Landult-Bornstein New Series group III, Pt a, Springer, Berlin, **22**, **(1982)**.
[18] R.Gangadharan, V.Jayalakshmi, J.Kalaiselvi, R. Murugan, B.Palanivel; Journal of Alloys and Compounds, **359**, 22 (**2003**).
[19] J.E.Jaffe, R.Pandey, M.Seal; J.Phys.Rev.B, **41**, 2876 **(1993)**.
[20] A.Nazzal, A.Qteish; Phys.Rev.B, **53**, 8262 **(1996)**.
[21] A.Qteish, M.Parrinello; Phys.Rev.B, **61**, 6521 **(2000)**.
[22] P.E.Camp, V.E.Doren, J.L.Martins; Phys.Stat.Sol., **190(1)**, 193 **(1995)**.
[23] P.Cortonay, P.Masriz; J.Phys.Condens.Matter., **10**, 8947 **(1998)**; P.Cortona, M.A.Villafiorita, P.Becker; Int.J.of Quantum Chem., **56(6)**, 831 **(1995)**.
[24] Z.J.Chen, H.Y.Xiaa, X.T.Zua; Physica.B., **391**, 193 **(2007)**.
[25] J.Yi, J.Lee, W. Song, Thin Solid Films, **431-432**, 349 **(2003)**.
[26] C.R.Sekhar, M.K.Karanjai; Thin.Solid Film, **322**, 117-122 **(1998)**.
[27] N.Fitzer, A.Kuligk, R.Redmer; Phys.Rev.B., **67**, 201201(R) **(2003)**.
[28] A.Shaukat, Y.Saeed, N.Ikram, H.Akbarzadeh; Eur.Phys.J., **B62**, 439-446 **(2008)**.
[29] F.Wooten; 'Optical properties of Solids', Academic Press, New York, **(1972)**.
[30] Y.H.Yu, S.C.Lee, C.S.Yang, C.K.Choi, W.K.Jung, J.Korean Phys.Soc., 682 **(2003)**.
[31] M.Belhadj, A.Tadjer, B.Abbar, Z.Bousahla, B.Bouhafs, H.Aourag; Phys.Stat.Sol., **241(11)**, 2516 **(2004)**.